Christoph Brandes, Marieke Hoog Antink, Stephen Kroll, Laura Treccani, Kurosch Rezwan

Aluminium acetate as alternative cross-linker for temperature controlled gel-casting and joining of ceramics

Journal Article as: peer-reviewed accepted version (Postprint)

DOI of this document*(secondary publication): 10.26092/elib/2483

Publication date of this document: 08/09/2023

* for better findability or for reliable citation

Recommended Citation (primary publication/Version of Record) incl. DOI:

Christoph Brandes, Marieke Hoog Antink, Stephen Kroll, Laura Treccani, Kurosch Rezwan,
Aluminium acetate as alternative cross-linker for temperature controlled gel-casting and joining of ceramics,
Journal of the European Ceramic Society, Volume 36, Issue 5, 2016, Pages 1241-1251, ISSN 0955-2219,
https://doi.org/10.1016/j.jeurceramsoc.2015.12.011.

Aluminium acetate as alternative cross-linker for temperature controlled gel-casting and joining of ceramics

Christoph Brandes[a], Marieke Hoog Antink[a], Stephen Kroll[a,b], Laura Treccani[a,*], Kurosch Rezwan[a,b]

[a] Advanced Ceramics, University of Bremen, Am Biologischen Garten 2, 28359 Bremen, Germany
[b] MAPEX-Centre for Materials and Processes, University of Bremen, 28359 Bremen, Germany

ARTICLE INFO

Article history:
Received 26 October 2015
Received in revised form
10 December 2015
Accepted 12 December 2015
Available online 24 December 2015

Keywords:
Gel-casting
Ceramic joining
Ionotropic gelation
Gel-forming rheology
Microstructure

ABSTRACT

In an earlier established gel-casting process, the biopolymer alginate is cross-linked with Ca^{2+}-ions released through the temperature controlled dissolution of calcium iodate-particles ($Ca(IO_3)_2$). In this study, aluminum acetate (AlAc) is compared to $Ca(IO_3)_2$ as an alternative temperature controlled cross-linker for an alginate–alumina slurry. Both cross-linkers are characterized regarding gel-forming properties, resulting microstructure, impurities, mechanics of sintered parts and the ability of joining ceramic blocks in the green state via connecting gelation with and without adding slurry. Rheological measurements show that both cross-linker have a similar gelling behavior and lead to gelled blocks of high quality. AlAc-particle create a denser and more homogenous microstructure, while $Ca(IO_3)_2$-particles induce pores, abnormal grain growth and lower mechanical values. Nevertheless $Ca(IO_3)_2$ shows excellent joining properties which makes it a suitable alternative to pressure joining. In summary, AlAc is an excellent alternative cross-linker but $Ca(IO_3)_2$ remains the method of choice for joining gelled bodies.

1. Introduction

Various types of gel-casting processes have been studied over the last decade and they are more and more frequently used for fabricating complex ceramic parts because of their advantages regarding processing time and shape complexity [1–4]. One of the most outstanding gel-casting processes is based on the ionotropic gelation of the biopolymer alginate. Ionotropic gelation of alginate-ceramics bases on the cross-linking between the guluronic acid-blocks of the heteropolymer alginate with multivalent cations (typically Ca^{2+}) [5,6]. This method is highly versatile and a wide range of shaping routes can be used. Among the calcium release methods, the temperature controlled release of Ca^{2+} from calcium iodate ($Ca(IO_3)_2$) is considered the best applicable. This method uses the rapidly increasing solubility of $Ca(IO_3)_2$ and the corresponding release of Ca^{2+}-ions with temperature [7].

Gelation of an alginate slurry with $Ca(IO_3)_2$ has been successfully used for casting complex shaped ceramics [8], extruded ceramic membranes [9]. Additionally, calcium-induced alginate gelation was successfully used for oxide ceramics (e.g., alumina, zirconia) [10–12] and non-oxide ceramics (e.g., ZrB_2–SiC, WC) [13,14]. These examples show that $Ca(IO_3)_2$ is an ideal choice for cross-linking complex shaped ceramics with almost no limitations regarding processability and sample geometry. The main disadvantage of all calcium-triggered ionotropic gelation techniques is the presence of other elements/ions from the cross-linking source besides calcium. For instance, additional elements such as phosphor, sulphur and iodine which derive from $Ca(PO_4)$ [10], $CaSO_4$ [15] and $Ca(IO_3)_2$ [16] respectively, have an impact on the final performance of the fabricated ceramics. The presence of such impurities typically negatively influences the properties of most ceramics, e.g. inhomogeneities, uncontrolled grain growth, sintering behavior and mechanical properties [17–20]. Therefore, it is necessary for a wider range of applications to find an alternative cross-linking source without the presence of additional elements or impurities. However, the alternative cross-linking source must feature the same good gel-forming quality and processability of $Ca(IO_3)_2$.

In general, the choice of a cross-linker is mainly dictated by the composition of the envisaged ceramic. For instance for aluminum compounds (e.g., alumina, zirconia toughened alumina, mullite, spinel, aluminum carbide) a promising, optional cross-linker is aluminum acetate (AlAc). Al^{3+}-ions serve a cross-linker and the acetate-ions as an organic compound are easily removed by

* Corresponding author. Fax: +39 035 0779653.
E-mail address: treccani@petroceramics.com (L. Treccani).

http://dx.doi.org/10.1016/j.jeurceramsoc.2015.12.011

thermal treatment which avoids undesired impurities. Previous works have shown that Al^{3+} can bind alginate chains almost as good as Ca^{2+} [21,22]. This suggests that AlAc is an ideal gelling agent for ionotropic gelation in ceramic process technology. However, the solidification of alginate ceramic slurries at room temperature (RT) with AlAc takes up to 11 h [23] and temperature induced gelation with AlAc has not been investigated so far, although the advantages for fast temperature controlled gelation are obvious. This can be seen for $Ca(IO_3)_2$, where the gelation time can be adjusted via temperature control from only a few minutes to several hours [24].

In this study two cross-linkers for alginate-based ionotropic gelation, $Ca(IO_3)_2$ and AlAc, are used to produce alumina parts by a temperature controlled route. The influence of both cross-linkers on the gelation behavior of the slurries and resulting microstructure and mechanical properties of the finally sintered parts is investigated in detail. Temperature ramp controlled oscillation rheology is used to compare the gelation behavior of the two cross-linkers during slurry fabrication, while ceramography and four-point bending tests (4-PB) are used for investigation of morphology, microstructure and mechanics. Additional to the processing and mechanical properties, the possibility to apply this process for joining green bodies is also investigated. By exploiting the more rapid binding of Ca^{2+}-ions to the alginate chains, individual parts are joined by bringing in contact gelled blocks. The possibility to use this method for rapidly fabricating more complex ceramic parts without additional pressure is considered. The quality of joining is assessed by characterizing the failure behavior and the characteristic strength of joined ceramics with 4-PB and compared to single block References.

2. Experimental procedure

2.1. Materials

For the slurry preparation α-alumina powder was purchased from Krahn Chemie GmbH, Germany (TM-DAR, particle size ~200 nm, purity 99.99%, Lot.: 9105). Ammonium hydroxide (NH_4OH, Product No: 30501, Lot.: SZBB0250) and 5-sulfosalicylic acid dihydrate (SSA, Product No: 52130, Lot: BCBK0642V) obtained from Sigma–Aldrich Chemie GmbH, Germany, are used as pH adjuster and dispersing agents. The cross-linkers calcium iodate ($Ca(IO_3)_2$, Product No: 30501, Lot.: MKBC8376V) and aluminum acetate dibasic (AlAc Product No.: 289825, Lot.: BCBN0146V) as well as the alginic sodium salt from brown algae acting as gelling agent (alginate medium viscosity, Product No.: 2033, Lot.: 051M0054V) were purchased from Sigma–Aldrich Chemie GmbH, Germany, while Protanal LFR 5/60 sodium alginate (Lot.: H10673) was obtained from FMC Biopolymer USA. Double deionized water (ddH_2O) with an electrical resistance of 18 MΩ (Synergy®, Millipore, Germany) was used for all experiments. All chemical were used as received.

2.2. Particle characterization of used cross-linkers

Scanning electron microscopy (SEM Supra 40 Zeiss, Field emission, Germany) was applied to analyze the particle size and morphology of $Ca(IO_3)_2$- and AlAc-particles. SEM analysis was carried out without any conductive coating.

2.3. Slurry preparation

The slurry was prepared using a protocol adapted from Brandes et al., [9]. In short, 1.2 g alginate (0.6 g of each alginate type) were dissolved in 50 ml ddH_2O (solvent) at RT and mixed for 30 min at 300 rpm (IKA Rw20.n, Staufen, Germany). The pH was set at pH 9 adding dropwise NH_4OH. To ensure a better viscosity the Al_2O_3-particles (180 g) were premixed with SSA (0.6 wt%) and slowly added to the alginate solution under continuous stirring for 1.5 h at 1900 rpm and RT for obtaining agglomerate-free alumina slurries. To reduce frictional heating and water evaporation, the slurry was kept in a cooling bath (~4 °C). Afterwards, the slurry (~48 vol.% solid content) was cooled in a fridge until its temperature was below 10 °C.

2.4. Casting and gelation

The cooled slurry was degassed (60 mbar) in a temperature controlled (10 °C) vacuum dispersion system (Dispermat LC2, VMA-Getzman, Germany) at 4000 rpm for 10 min. In the following step, 5.5 mmol of the cross-linker (~2 g $Ca(IO_3)_2$ or ~0.9 g AlAc) was admixed at the same pressure and stirring velocity. As shown in Fig. 1A, the slurry was casted into rectangular block molds made of LEGO® basic bricks (brick type 2 × 4, width and depth: ≈25 mm; height: small mold composed of 4 bricks ≈36 mm, large mold composed of 8 bricks ≈64 mm). The molds were sealed with polytetrafluorethylene (PTFE) to prevent drying of the samples during the subsequent heating process. After filling and sealing, the molds were placed in a temperature controlled humidity chamber for 15 min at 45 °C and 80% relative humidity (KBF, Binder, Tuttlingen, Germany). For the two applied joining processes (Fig. 1B), namely slurry joining and contact joining, two small gelled blocks were used. In the slurry joining process, slurry and cross-linker were mixed as previously described for the sample block fabrication. Here, approximately 0.2 ml of slurry was spread on each contact surface of the small blocks with a spatula before placing the blocks on top of each other. For the contact joining process the small gelled blocks were directly placed on top of each other. Both types of joined blocks were stored in the climate chamber (45 °C, 80% relative humidity) for further 15 min until demolding. Afterwards, all samples were dried for two days at 25 °C and 90% relative humidity followed by final drying for two days at 20 °C and 50% relative humidity.

Each prepared block was cut with a wire saw (Well™ 6234, Mannheim, Germany) to obtain 9 bending specimens (Fig. 1C). The specimens were ground and finally sintered at 1500 °C for 2 h (Nabertherm HT0817, Lilienthal, Germany), using a heating rate of 500 °C/h. Due to the low amount of alginate (0.6 wt.%), no extra debinding step was necessary.

2.5. Small deformation oscillation rheology

To analyze the samples' viscoelastic properties during gelation, small deformation oscillatory measurements of storage modulus (G′) and loss modulus (G″) were conducted (Discovery Series Hybrid Rheometer HR3, TA Instruments) with a plate–plate geometry (ø = 40 mm). The gap distance, strain and frequency were set to 1 mm, 0.2% and 1 Hz, respectively. Prior to each measurement, the cooled slurry (10 °C) and the cross-linker were directly mixed and 1.1 ml of slurry was placed between the plates with a syringe. To simulate the warming of the slurry during handling and temperature controlled gelation a heating rate of 1 °C/min and a starting temperature of 10 °C were selected. This is in conformity with the measured warming inside a sample during the manufacturing and gelation process. The dissipation factor tan(δ) was calculated from loss modulus (G′) and storage modulus (G″) to determine the degree of cross-linking on the ideal elastic behavior.

2.6. Surface analysis of the gelled green bodies

Surface roughness (Ra) of gelled blocks derived from each type of cross-linker ($Ca(IO_3)_2$ versus AlAc) was determined using

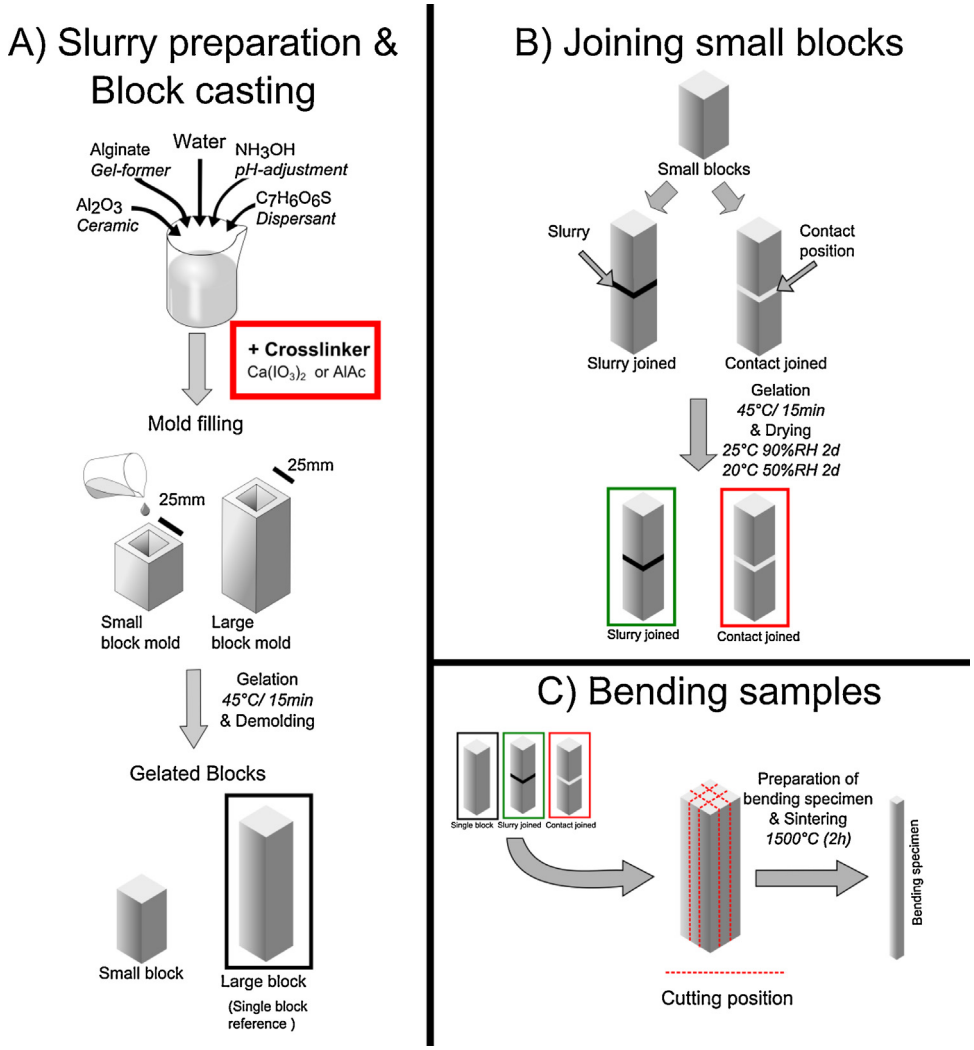

Fig. 1. (A) Schematic overview of the slurry preparation and casting process of gelled blocks. (B) Schematic overview of the production of slurry joined and contact joined samples. (C) Preparation of the bending test specimen used for 4-point bending tests.

3D-profilometry (Plμ 2300, Sensofar Technology, Terrassa, Spain) according to ISO 4287 [25]. Samples were imaged using a 20× objective lens, equivalent to an area of $900 \times 1200\ \mu m^2$. For statistical significance, five measurements at different positions were taken for each gelled block surface shortly after demolding.

2.7. Analysis of the sintered samples

2.7.1. Ceramography

The geometrical density of the alumina powder and prepared samples was measured with a He-pycnometer (Pycnomatic ATC, Porotec) to calculate the relative density.

The connectivity at the joining position of all sintered samples was investigated by SEM to visualize potential macro- and microdefects.

Grain size measurements were performed after thermal etching using electron microscopy (SEM Supra 40 Zeiss, Field emission, Germany) according to DIN EN 623-3 [26]. Each sample was therefore prepared by grinding (diamond disc providing 30 μm grain size), lapping (lapping disc providing 9 μm grain size), polishing (perforated synthetic fiber cloth providing 3 μm grain size) and final thermal treatment at 1300 °C for 1 h in air according to [27]. The atomic content of calcium and iodine was determined by X-ray energy-dispersive spectrometry (EDS) (Bruker XFlash 6|10, USA).

X-ray diffraction (XRD) was conducted with a Seifert XRD powder diffractometer (ID 3303 research edition, General Electric, USA) using Cu-Kα radiation. Diffractograms were detected from 2-θ = 10 to 80° with a stepscan of 0.25° and a dwelling time of 5 s. Powder diffraction files (PDF) from the International Centre of Diffraction Data (ICDD) were used to identify the crystal phases.

2.7.2. Mechanical characterization by 4-point bending tests: joined blocks versus reference blocks

The flexural strength of the prepared samples was measured in accordance with DIN EN 843-1 [28] using four-point bending tests (4-PB) (Zwick Z005, Germany). 4-PBs were applied to quantify the breaking position within the joined blocks compared to a reference composed of one large block element. Therefore, histograms of the breaking positions were generated using 2 mm intervals for evaluation. Furthermore, Weibull distributions of the flexural strength were determined for joined blocks and reference bulk samples. For 4-PBs a measurement set up recommended by the norm was used (inner span = 20 mm, outer span = 40 mm, testing speed = 0.5 mm/min, specimen size = 3 × 4 mm and specimen length >42 mm, n = 30 specimens for each sample type if not otherwise mentioned). After the blocks broke, the breaking position was marked and the applied force necessary for sample failure was noted.

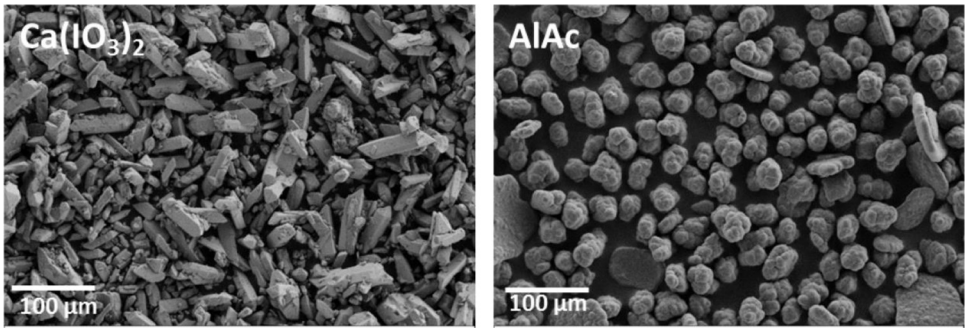

Fig. 2. SEM micrographs of the different particulate cross-linkers used for ionotropic gelation: $Ca(IO_3)_2$ (left) and AlAc (right) used as cross-linker source.

3. Results

3.1. Morphology and size of used particulate cross-linkers

Fig. 2 shows two SEM micrographs of the used $Ca(IO_3)_2$- and AlAc-particles as received. The images show that both $Ca(IO_3)_2$- and AlAc-based cross-linkers have an average diameter between ~20 μm and ~50 μm, but a different particle morphology. $Ca(IO_3)_2$-particles have a euhedral, long, thin, almost needle-like morphology, while the AlAc-particles appear more rounded and platelet type agglomerates.

3.2. Small deformation oscillation rheology

The measured rheology results of the gelation behavior of $Ca(IO)_3$-compared to AlAc-treated slurries are plotted in Fig. 3. Fig. 3A shows that loss modulus and storage modulus increase over time and rising temperature (Fig. 3C) from 10 to 30 °C within 20 min. The storage modulus is in both cases about 10-times higher than the corresponding loss modulus and increases by a factor of 10 (2–20 MPa) during the measurement time. Fig. 3B shows the dissipation factor tan(δ), the ratio of G″/G′, for both cross-linkers. It can be seen that the value drops rapidly in the first 5 min. This time corresponds to the time necessary for mold filling and mold sealing. After 5 min, tan(δ) slowly decreases until it reaches 0.082 and 0.098 for AlAc and $Ca(IO_3)_2$, respectively, at the end of the gelation process (i.e., after 20 min). Fig. 3C shows the applied temperature profile of the measurement and the measured temperature inside of a sample during handling and gelation. The applied temperature ramp started at 10 °C and increases with ~1 °C/min up to 30 °C.

3.3. Structural characterization of green and sintered samples: slurry and contact joined blocks compared to single reference blocks

For both cross-linker systems the dried green bodies of slurry and contact joined samples in comparison to single reference blocks are presented in Fig. 4A. Macroscopic defects can only be seen for contact joined AlAc-based samples. These samples show discontinuous connections and small gaps at the joining position. All other samples are apparently well connected and macroscopic gaps or transitions between the blocks are not obvious. On the microscopic scale (Fig. 4B) the $Ca(IO_3)_2$-based single block shows pores in the range of 20–200 μm distributed over the whole sample leading to a reduced apparent density. Similar sized pore inclusions can be found in the slurry joined and contact joined $Ca(IO_3)_2$-based samples. A slight increase in the amount of pores and defects in the area of the joining position can be seen. The initial connectivity reduces for $Ca(IO_3)_2$-treated specimens from 95% (single block and slurry joined) down to 90% for a contact joined specimen (Table 1). In this case connectivity is defined as the percentage solid content in the joining area or its corresponding position in the single block. The AlAc-single block as reference sample shows no pores. Porous defects (>200 μm) are existent in the slurry joined and contact joined samples near to the joining area. The presence of such defects reduces the initial connectivity from 95% down to 85% and 65% for slurry and contact joined samples, respectively. At a higher resolution the microstructure shows that within one cross-linker type the grain sizes are constant (Table 1), but differences between the two cross-linker types become visible. The samples prepared with $Ca(IO_3)_2$ show a wider size range and a higher average grain size (~1100 nm) compared to AlAc-based samples. Partially abnormal grain sizes can be found showing grain sizes 3–4 times higher than the average grain size. AlAc-based samples show a more homogenous microstructure with a smaller grain size (~900 nm) and more regular grain size distribution.

According to XRD analysis shown in Fig. 5A, only α-alumina related peaks are found in $Ca(IO_3)_2$-based and AlAc-based single block samples after sintering at 1500 °C for 2 h. Other crystalline phases are not detected.

Furthermore, qualitative EDX-mapping shows the concentration of calcium at the examined position (Fig. 5B) where the concentration of calcium correlates with the red intensity. It can be seen that the highest intensity, and therefore the highest calcium concentration, is located around the pores (Fig. 5B, bottom left). Table 2 shows the measured elemental concentrations of aluminum, oxygen, calcium and iodine for a $Ca(IO_3)_2$-based sample. The concentration of iodine was below the detection limit (≤0.4 wt%).

Table 1
Grain size analysis according to DIN EN 623-3 [26] and estimated connectivity of the samples bases on porosity measurement (He-pycnometer) or microscopic image analysis.

Cross-linker	Sample system	Grain size (nm)	Estimated connectivity at the joining position (%)
$Ca(IO_3)_2$	Single block	1141 ± 203	95[a]
	Slurry joined	1088 ± 217	95[a]
	Contact joined	1160 ± 253	90[b]
AlAc	Single block	878 ± 117	97[a]
	Slurry joined	912 ± 263	85[b]
	Contact joined	882 ± 88	65[b]

[a] Based on porosity measurements using He-pycnometer.
[b] Based on microscopic image analysis.

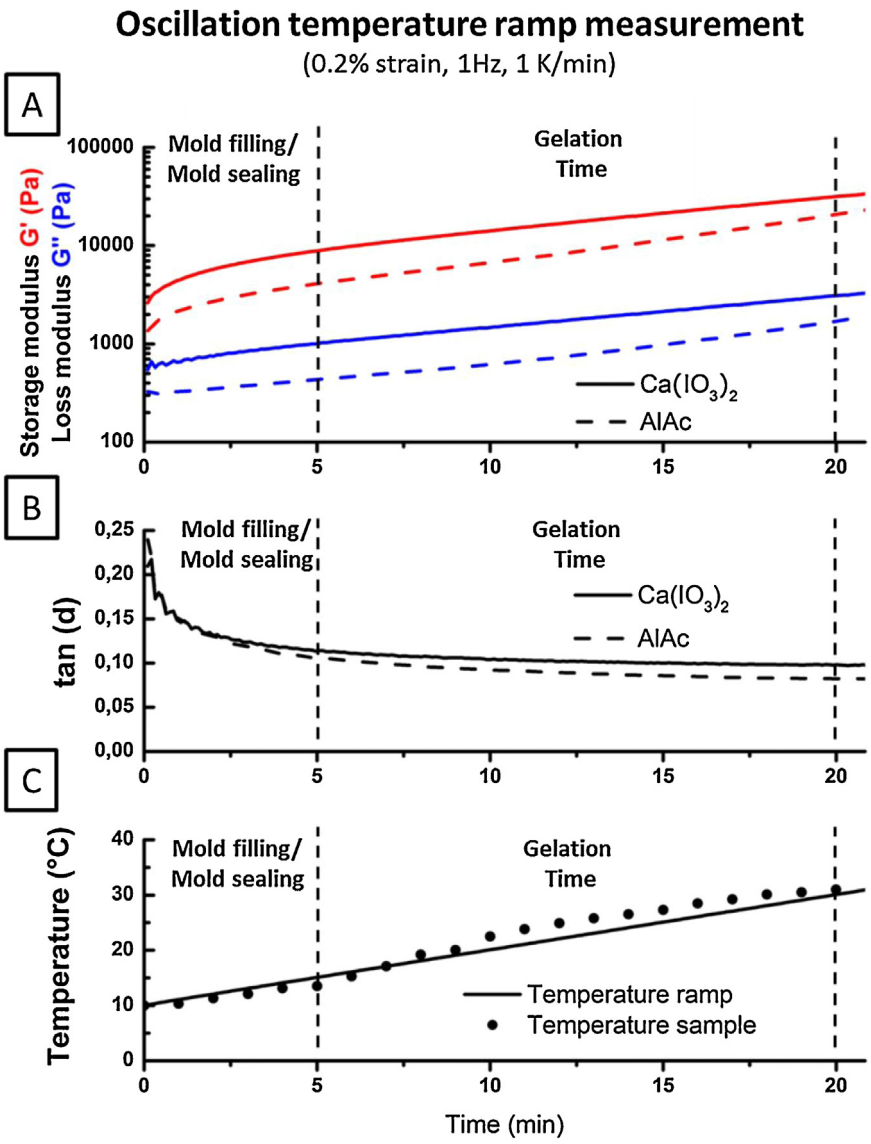

Fig. 3. (A) Mechanical spectra (0.2% strain, 1 Hz) showing variation of G′ (red) and G″ (blue) of slurries containing $Ca(IO_3)_2$ (continuous line) and AlAc (dotted line) cross-linkers as a function of time. (B) The corresponding ratio of G′ and G″ indicated as tan(δ) is plotted in dependency of the time. (C) The oscillation rheology measurement was performed with a simultaneous heating rate (line) of 1 °C/min, starting at 10 °C in accordance with the measured warming inside a sample (dots). (For interpretation of the references to color in this figure legend, the reader is referred to the web version of this article.)

3.4. Mechanical characterization of sintered samples: joined blocks versus reference blocks

For the joining of the samples the quality of the connecting surfaces is a relevant aspect to be considered. In relation to both cross-linker systems the fresh gelled surfaces show small unevenness indicated by 3D-profilometry (Figure S1 A). As determined by extracted 2D-line scans they extend over several square micrometer (Fig. S1 B) and result for both preparation methods in a similar average surface roughness of 2.8 μm ($Ca(IO_3)_2$) and 2.7 μm (AlAc), respectively.

Supplementry material related to this article found, in the online version, at http://dx.doi.org/10.1016/j.jeurceramsoc.2015.12.011.

The results of the 4-PB test are given in Fig. 6 showing schematically the experimental set-up (A), the histograms of the breaking position (B) and the Weibull distribution diagrams (C) for both cross-linker systems compared to single reference blocks. To evaluate the failure behavior within the inner span (20 mm length), all specimens are divided into 10 intervals with a length of 2 mm each (Fig. 6A). For both cross-linker systems $Ca(IO_3)_2$ and AlAc the percentaged frequencies for failing (FF) within an interval are plotted as histograms and the failure behavior of joined blocks (slurry versus contact joined) and reference sample is contrasted (Fig. 6B) The intervals from 8 to 10 mm and 10 to 12 mm correspond to the joining area. Every measured sample has a share of ≈3.3% FF and this leads, under the assumption of an evenly distributed breaking position, to the expected value of 10% for each interval. The results show that the $Ca(IO_3)_2$-single block has no conspicuously increased

Table 2
Element concentration measured via EDX for single reference blocks fabricated using the cross-linker system $Ca(IO_3)_2$.

Element	Norm. (wt.%)
Al	48.27 ± 1.24
O	47.94 ± 3.78
Ca	3.79 ± 0.24
I	–

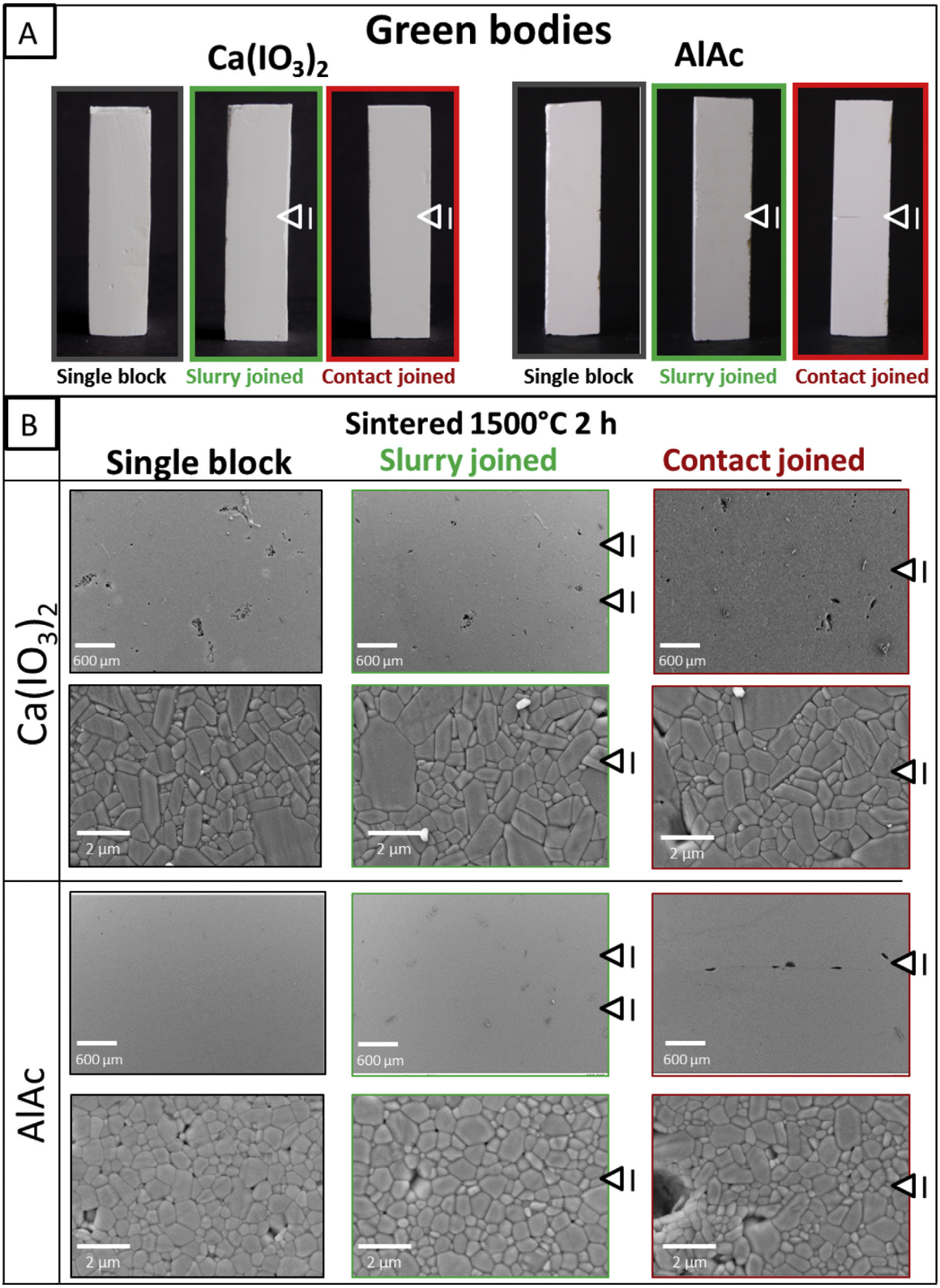

Fig. 4. (A) Comparison of slurry joined and contact joined green body samples of the $Ca(IO_3)_2$ and AlAc route with single block reference (no joining) after drying step. The joining position of slurry and contact joined samples is marked with an arrow. (B) Cross sectional SEM micrographs of the sintered contact area at the joining position (slurry and contact joined) or at the equivalent sample height (single reference block) for both cross-linker systems. The top rows show a larger overview while the bottom rows show the polished and thermally etched microstructure.

probability of failure in the joining region (total 10% FF). The slurry joined $Ca(IO_3)_2$ sample shows a FF of 20% in the interval between 8 and 10 mm, but in the interval 10–12 mm the FF is below average (6.6%). In contrast, the contact joined $Ca(IO_3)_2$ sample shows a total sum of failure of 60% in the joining area, a significant higher FF than the two other $Ca(IO_3)_2$-based samples. The histogram of the AlAc-

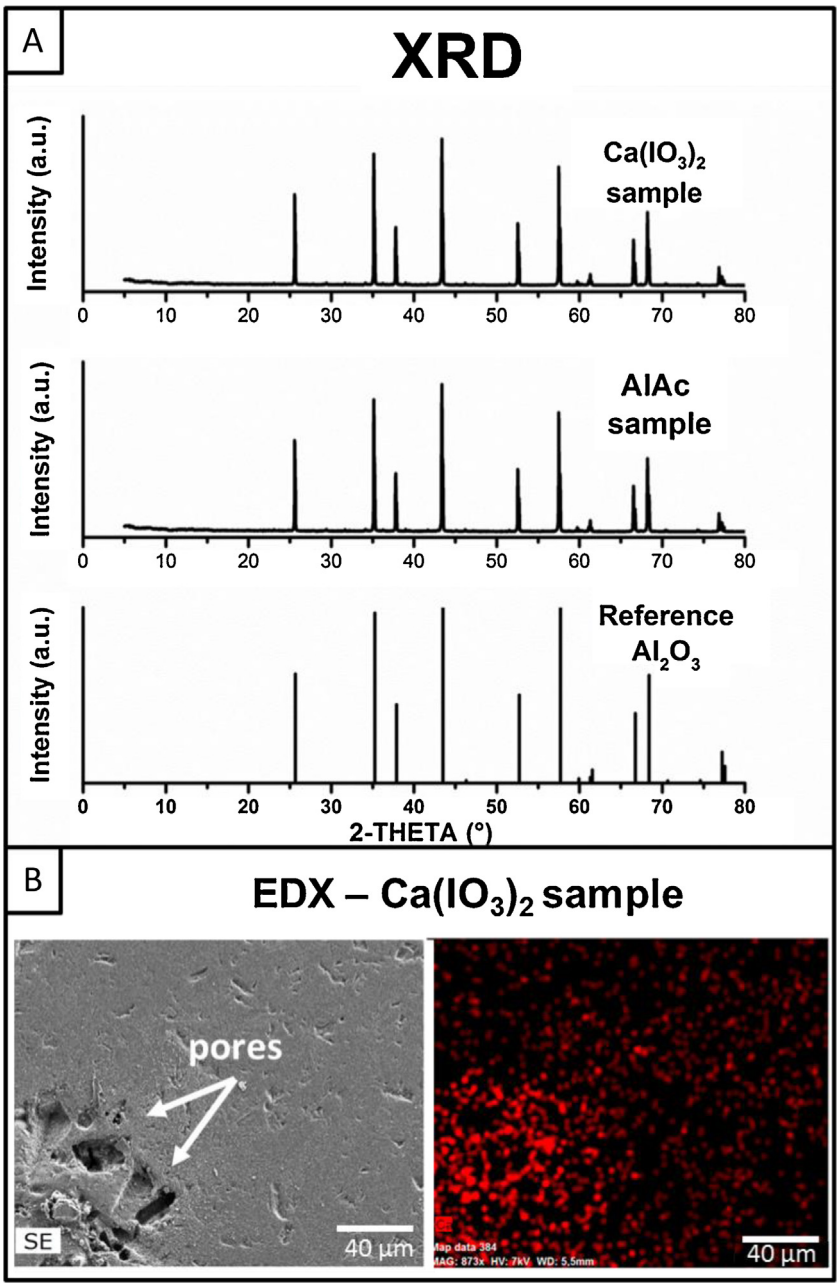

Fig. 5. (A) XRD diffractograms of $Ca(IO_3)_2$- and AlAc-based samples (single reference blocks) after sintering at 1500 °C for 2 h and the pure α-alumina reference. (B) SEM micrograph (left) and corresponding EDX mapping (right) showing the calcium distribution indicated as red spots. (For interpretation of the references to color in this figure legend, the reader is referred to the web version of this article.)

single reference block shows slightly increased values in the range from 4 to 14 mm compared to the $Ca(IO_3)_2$-based single reference block. However, an overall FF in the area of joining is not obvious. In contrast, for the slurry joined and contact joined AlAc-sample an increased FF in the joining area is evident and the total failure probability is 60% and 73%, respectively.

Fig. 6C shows the Weibull distribution diagrams for all different types of samples. The AlAc-single reference block has the highest flexural strength (σ_0 = 324 MPa) and Weibull modulus (m = 9.9), while the $Ca(IO_3)_2$-based reference shows significantly lower values (σ_0 = 263 MPa, m = 8.0). However, concerning the different joining techniques, different behaviors of the two applied cross-linkers are observed. The slurry joined $Ca(IO_3)_2$ sample reaches a maximum flexural strength (σ_0 = 259 MPa) similar to the $Ca(IO_3)_2$-single reference block (σ_0 = 263 MPa), but the strength distribution is more unsteady and reduces the Weibull modulus m to 6.2. A similar effect can be seen for the contact joined $Ca(IO_3)_2$ samples. Here, a more distinct variation of the strength values in a range between 85 and 285 MPa is observed. Compared to the reference block the flexural strength (σ_0) and Weibull modulus (m) decrease to 239 MPa and 3.3 respectively. The same effect is more evident for the slurry and contact joined AlAc-based samples. The highest flexural strength of the slurry joined sample (~360 MPa) is similar to the reference material, but with a larger variation in values from 120 to 360 MPa. This is far more pronounced than for the $Ca(IO_3)_2$-based samples featuring a flexural strength of σ_0 = 272 MPa and a Weibull modulus of m = 3.7. The contact joined AlAc sample shows the weakest mechanical value

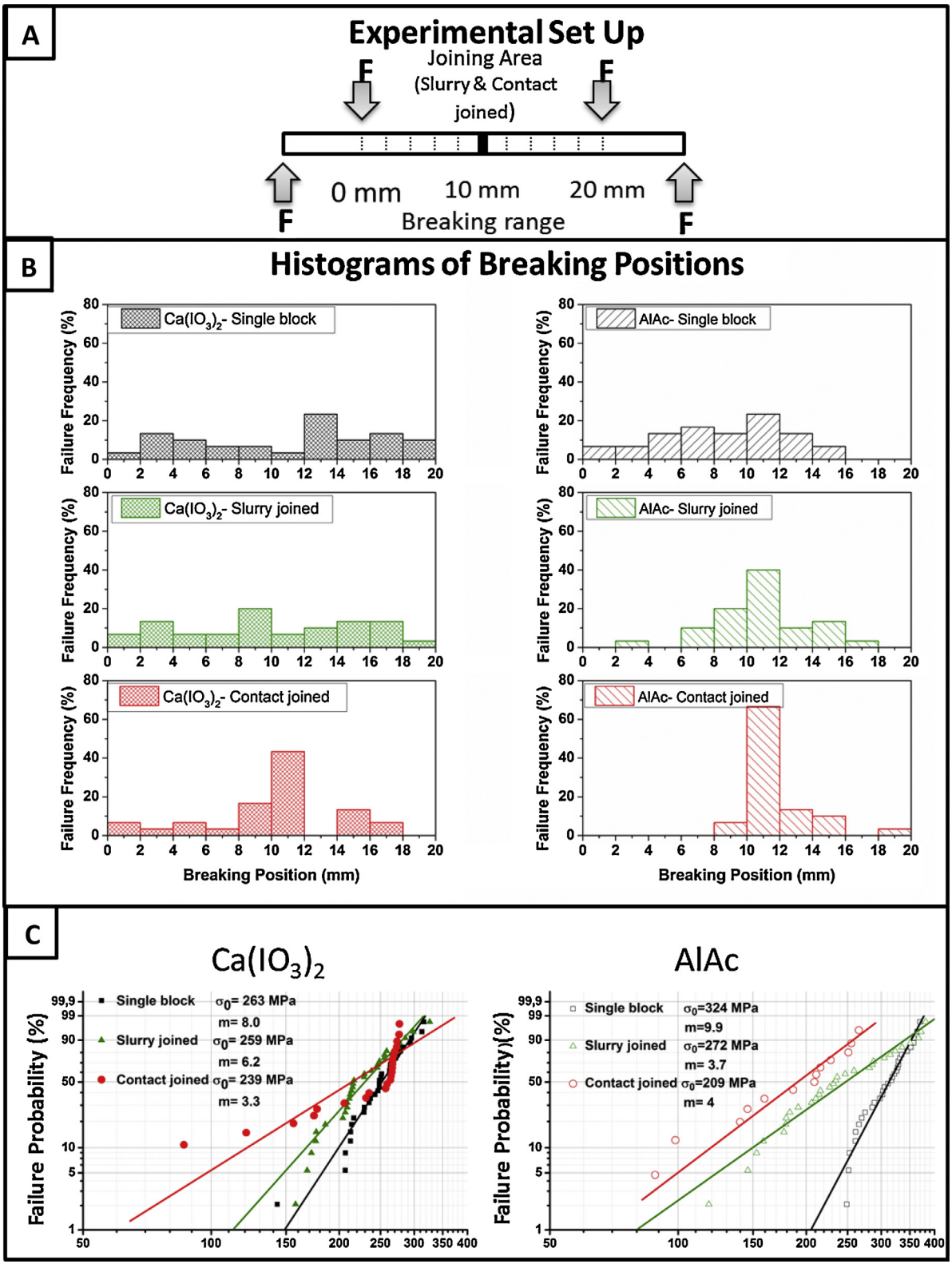

Fig. 6. (A) Schematic experimental set-up for the used 4-PB. The breaking positions of all samples were classified into 2 mm intervals. (B) Histogram evaluations of the breaking positions for slurry and contact joined samples in dependence on the used cross-linker system compared to single reference blocks. (C) Weibull distribution diagrams summarizing the flexural strength (σ_0) and Weibull moduli (m) for the different sample fabrications (single block, slurry and contact joined samples).

of σ_0 = 209 MPa. The specimens partially broke prior to the measurement or during preloading, and were not used for mechanical evaluation (n = 17 specimens). The maximum strength (260 MPa), flexural strength σ_0 (209 MPa) and Weibull modulus m (4.0) calculated from the obtained results are particularly lower compared to all other tested samples. Both the flexural strength values (σ_0) as well as the Weibull moduli (m) are summarized in Table 3.

Table 3
Overview of the characteristic flexural strength values (σ_0) and Weibull moduli (m) measured via 4-PB.

Cross-linker	Sample system	Flexural strength (MPa) σ_o	Weibull modulus (m)
$Ca(IO_3)_2$	Single block	263	8.0
	Slurry joined	259	6.2
	Direct joined	239	3.3
AlAc	Single block	324	9.9
	Slurry joined	272	3.7
	Direct joined	209	4.0

4. Discussion

4.1. Gel-forming process

The results show that in the temperature controlled process both $Ca(IO_3)_2$ and AlAc have a similar gel-forming and solidifying behavior. For instance, both prepared alumina-based slurries have the same good processability and similar rheological properties within a working time of 20 min. This indicates that both cross-linkers have a similar temperature dependent dissolution behavior. Laucournet et al., [29] describe the solubility and coagulation of alumina particles with AlAc under thermal treatment. According to their study, the solubility of AlAc increases by a factor of ~2 when temperature increases from 25 °C to 35 °C. For a larger temperature rise (from 10 °C to 30 °C) a higher increase in solubility is likely. This solubility increment of AlAc is in the same region as for $Ca(IO_3)_2$, whose solubility increases by a factor of ~3 if the temperature is increased from 10 °C to 30 °C [7]. Besides the gel-forming, $Ca(IO_3)_2$ and AlAc lead to additional solidification via particle coagulation [29,30]. Particle coagulation is related to the increase of ion concentration and a pH-shift derived from further cross-linker dissolution [31]. Because of their identical solubility increase and working mechanisms both cross-linkers induce fully gelled green bodies in the temperature controlled process and in short time.

It has been observed that the green bodies gelled with AlAc are stiffer, less flexible and more brittle, which indicates a stronger cross-linking between the alginate chains. This is also supported by the lower dissipation factor tan(δ) for the AlAc-gelation than for the $Ca(IO_3)_2$-gelation. In general, materials with a lower dissipation factor are closer to an ideal elastic body [32]. In our alginate systems the loss of viscous behavior can only be reached by a stronger cross-linking between the alginate chains. The increased cross-linking effect could be a result of a better binding of triple charged Al-ions (Al^{3+}) in comparison to double charged Ca-ions (Ca^{2+}) [22].

4.2. Ceramography

Despite the widespread use of $Ca(IO_3)_2$ as cross-linker for ceramic slurries [16,8,9], the effects of its dissolution and the influence of released ions (Ca^{2+} and I^-) on the bodies morphology and microstructure of gel-casted ceramics have not been reported yet. Our results shows that the presence of $Ca(IO_3)_2$ does not lead to the formation of a second crystalline phase next to alpha-alumina. Although the formation of other crystalline phases such as calcium oxide, Ca—Al—O compounds or iodine containing phases is likely, these were not observed. In order to determine the qualitative concentration and distribution of calcium and other ions EDX combined with electron microscopy was used. The EDX results (Fig. 3B) qualitatively describe the non-homogenous spread of calcium through the whole sample and a higher calcium concentration around pores. The irregular spreading of Ca-atoms is supposed to create inhomogeneities within the ceramic and e.g., lower the overall stability. The pore morphology and size at the sites of highest calcium concentration is similar to the size of the initial $Ca(IO_3)_2$-based particles (~20–50 μm). This indicates that $Ca(IO_3)_2$-crystals induce pore formation within the ceramic. Pore formation can be caused by the higher calcium concentration in proximity of the particle surfaces where the slurry starts to gel first. Due to the cross-linking, the slurry gels and the viscosity increases. Therefore, the slurry cannot replace for the space occupied by dissolving $Ca(IO_3)_2$-particles. This effect can explain the higher calcium concentration around the pores since most calcium is bound to the alginate in the area close to the initial $Ca(IO_3)_2$ crystals. A second effect that could lead to pore formation is the thermal decomposition of the $Ca(IO_3)_2$ during sintering. The iodate ions (IO_3^-) are thermally instable and break up at temperatures >300 °C. Thereby the resulting gases (I and O) outgas as the initial $Ca(IO_3)_2$-particles vanish. This effect would explain the low concentration of iodine in the ceramic below the detection limit of the EDX. Most likely both effects contribute to the pore formation. Equivalent investigations for the spreading of Al-ions from the cross-linker AlAc through the Al_2O_3-matrix are not possible due to the untraceability of Al in Al_2O_3. Nevertheless, pores which remain after sintering in shape of the initial crystals could not be observed in the AlAc-based reference. It is supposed that the absence of pores with AlAc single-block is related to the conversion of AlAc into Al_2O_3 during sintering or a slower AlAc dissolution and better diffusion into the slurry. One opportunity to reduce the negative effects of $Ca(IO_3)_2$ could be the use of smaller particles of higher surface area which can change the gelation by a faster dissolution compared to the used quantity of $Ca(IO_3)_2$ at the same temperature.

Another negative effect of the presence of large amounts of Ca-ions in Al_2O_3 is the enhanced and abnormal grain growth. Ca is known for influencing grain growth [33,34], especially if large amounts of Ca are required as for the presented processing route used in this study (3.8 wt.%). The observed increase of grain size from ~880 nm for AlAc to ~1100 nm for $Ca(IO_3)_2$ is evident and in agreement with previously performed microstructure analysis of Ca-doped alpha-alumina by Altay et al., [35]. Through the inhomogeneous distribution of Ca through the ceramic, the grain growth is inhomogeneous. Both partially abnormal grains and smaller and more homogeneous grains can be seen. This wider grain size distribution further increases the inhomogeneous properties of $Ca(IO_3)_2$-gelled samples compared to AlAc-gelled samples. The presence of pores together with an uncontrolled grain growth and a resulting inhomogeneous microstructure are the reasons for a mechanically weaker $Ca(IO_3)_2$-reference compared to the AlAc-reference (single reference blocks). The latter has a more regular, finer and denser microstructure with small grains.

4.3. Joining of ceramic green bodies

Despite the different microstructure, the joining mechanisms of gelled green bodies for both cross-linker systems are similar (Fig. 7A). Possibly not all guluronate acid groups (G) of the alginate present at the joining surface are fully saturated with Ca- or Al-ions (Fig.7B). If two surfaces with unsaturated chains get into contact, the alginate chains of the opposite surfaces can crosslink (Fig. 7C) and form one single body composed of two elements. Due to the elasticity of the gelled small blocks, surface unevenness can be leveled. The additional spreading of slurry between the blocks can further reduces the effect of surface unevenness and provide more cross-linking ions as well as unsaturated alginate chains.

The achieved results prove that in all cases the joining process was feasible. The alginate chains bind to each other and during the sintering process two small single blocks become one connected sample without applying additional pressure. The strength and quality of the binding differs for the methods and cross-linkers,

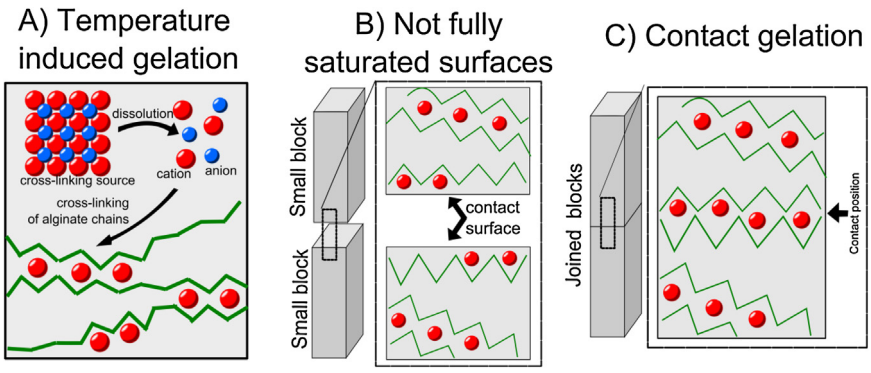

Fig. 7. Schematic overview of the joining principle. (A) The cross-linking source dissolves and the released cations cross-link the guluronate acid (G) sequences in the alginate chain (G). (B) The alginate chains at the surface are not full saturated with cross-linking ions. (C) When brought into contact the alginate chains at the surface can crosslink and form a single block.

but the overall stability of the joint induced by ionotropic gelation is given. To prove this method of joining surfaces, small blocks were brought in contact with saturated $CaCl_2$ or $AlCl_3$ solution. In both cases all alginate chains at the surface were saturated with ions and a successful joining process via slurry or contact joining was no longer possible (data not shown). However, the results of the 4-PB showed that the joining process leads to a higher failure rate at the joining position and the joined samples showed lower mechanical strength values compared the single block References

Based on the failure frequency at the joining position the slurry joined $Ca(IO_3)_2$-based samples show the best results. Compared to the corresponding $Ca(IO_3)_2$-single reference block the frequency of failure is only slightly increased and in addition, the flexural strength $\sigma_0 = 259$ MPa is close to the obtained flexural strength of the reference ($\sigma_0 = 263$ MPa).

Some $Ca(IO_3)_2$-based slurry joined specimens reached the same maximum strength values as the reference. The strength of a larger number of slurry joined specimens is shifted towards lower values without falling below the lowest measured strength of the $Ca(IO_3)_2$ reference. This shows that the slurry joining of two separate parts using $Ca(IO_3)_2$ is feasible without dramatic strength loss. On the contrary, AlAc slurry joining is less recommendable due to the lower Weibull modulus and higher probability of failure in the area of joining, unless predetermined breaking points are needed or the mechanical load is low. In general, contact joining is less effective than slurry joining: both cross-linkers lead to a weaker joining, indicated by the lower characteristic strength and the high FF in the joining area. This is mainly caused by the dissolved cross-linker particles or entrapped air voids of similar size. If the particle size-effect is predominant could be determined by the use of pre-milled powders with smaller particle sizes and analysis of the resulting pore sizes. Nevertheless, the joint created with $Ca(IO_3)_2$ is better than with AlAc, since less macroscopic defects appear.

The general better joining behavior of calcium can be related to the higher saturation of guluronic acid with calcium ions as confirmed by rheological investigation (Fig. 3). Also the levelling of the surface unevenness through the stiffer AlAc blocks is no longer possible. This leads to the conclusion that calcium might be in general the favored cross-linker for alginate since it is also the preferred element for cross-linking alginate chains in natural systems like brown seaweed [36].

Judging from the joining quality the $Ca(IO_3)_2$ method could be an alternative to other joining methods. Compared to pressure joining the alginate route is faster, does not require special preparation of surfaces and allows for more complex parts [37,38]. Compared to other slurry joining methods the alginate route shows advantages: it allows the fast joining of gelled blocks without pre-sintering parts or the creation of interlayers with different thermal-expansion or mechanical properties [39–41]. The process is also favorable to methods where hot gelatin slurries are used for casting and joining [42]. Alginate does not require hot slurries for its processability and it leads to similar mechanical values. Additionally, the method can be used for joining different ceramics or the creation of ceramics with gradients of pores or concentrations. However, the bending strength for the $Ca(IO_3)_2$-based samples is lower compared to the typical values for gel-casted alumina [43,44], but AlAc leads to similar values. Therefore, AlAc is more interesting for complex shaped ceramics with high loading applications, while $Ca(IO_3)_2$ is more suitable for joined parts with applied loading.

5. Conclusion

For the temperature controlled gelation of alginate ceramic slurries AlAc is a reasonable alternative to the standard $Ca(IO_3)_2$. It shows the same good processability as the Ca-compound, without the negative effects in the microstructure. Compared to $Ca(IO_3)_2$ AlAc leads to a more homogenous and less porous alumina-ceramic, while $Ca(IO_3)_2$ induces larger pores, grain growth and an inhomogeneous microstructure. These resulting effects have significant influence on the mechanical strength of the sintered materials. AlAc shows significantly better flexural strength (324 MPa) and possesses a higher Weibull modulus (9.9). Therefore the AlAc route is to prefer for the ionotropic gelation of aluminum-compounds. If joining of the ceramics in the green body state is required for the creation of more complex shapes $Ca(IO_3)_2$-slurry joining shows the best results. The simple process allows for a fast, pressure-free joining and compared to the reference almost the same mechanical values (~260 MPa) can be achieved. In summary, AlAc is the better alternative for gel-casting in joining processes, whereas $Ca(IO_3)_2$ remains the method of choice for joining ceramics in the green state.

Acknowledgements

We thank the European Research Council for financial support within the BiocerEng, Project No. 205509. We thank Thomas Schumacher (University of Bremen, Advanced Ceramics) for his support with the XRD analysis.

Appendix A. Supplementary data

Supplementary data associated with this article can be found, in the online version, at http://dx.doi.org/10.1016/j.jeurceramsoc.2015.12.011.

References

[1] O.O. Omatete, M.A. Janney, S.D. Nunn, Gelcasting: from laboratory development toward industrial production, J. Eur. Ceram. Soc. 17 (2–3) (1997) 407–413.
[2] M.Y. Huang, D.Q. Zhang, Z.H. Liu, J. Yang, F. Duan, C.K. Chua, S.C. Lim, M.S. Yip, Comparison study of fabrication of ceramic rotor using various manufacturing methods, Ceram. Int. 40 (8) (2014) 12493–12502.
[3] S. Leo, C. Tallon, N. Stone, G.V. Franks, Near-net-shaping methods for ceramic elements of (body) armor systems, J. Am. Ceram. Soc. 97 (10) (2014) 3013–3033.
[4] N.O. Shanti, D.B. Hovis, M.E. Seitz, J.K. Montgomery, D.M. Baskin, K.T. Faber, Ceramic laminates by gelcasting, Int. J. Appl. Ceram. Technol. 6 (5) (2009) 593–606.
[5] G.T. Grant, E.R. Morris, D.A. Rees, P.J.C. Smith, D. Thom, Biological interactions between polysaccharides and divalent cations: the egg-box model, FEBS Lett. 32 (2) (1973) 195–198.
[6] M.I. Nieto, I. Santacruz, R. Moreno, Shaping of dense advanced ceramics and coatings by gelation of polysaccharides, Adv. Eng. Mater. 16 (6) (2014) 637–654.
[7] P.A.S. Smith, Alkaline-earth metal halates, J. Am. Chem. Soc. 106 (10) (1984), 3068.
[8] Y. Jia, Y. Kanno, Z.P. Xie, Fabrication of alumina green body through gelcasting process using alginate, Mater. Lett. 57 (16,17) (2003) 2530–2534.
[9] C. Brandes, L. Treccani, S. Kroll, K. Rezwan, Gel casting of free-shapeable ceramic membranes with adjustable pore size for ultra- and microfiltration, J. Am. Ceram. Soc. 97 (5) (2014) 1393–1401.
[10] Y. Jia, Y. Kanno, Z.P. Xie, New gel-casting process for alumina ceramics based on gelation of alginate, J. Eur. Ceram. Soc. 22 (12) (2002) 1911–1916.
[11] T. Nozaki, T. Arima, K. Idemitsu, Y. Inagaki, Synthesis of zirconia sphere particles based on gelation of sodium alginate, J. Nucl. Mater. 412 (2011) 184–189.
[12] H. Akhondi, E. Taheri-Nassaj, A. Taavoni-Gilan, Gelcasting of alumina–zirconia–yttria nanocomposites with Na-alginate system, J. Alloys Compd. 484 (1,2) (2009) 452–457.
[13] R.J. He, R.B. Zhang, X.L. Zhu, K. Wei, Z.L. Qu, Y.M. Pei, D.N. Fang, Improved green strength and green machinability of ZrB2-SiC through gelcasting based on a double gel network, J. Am. Ceram. Soc. 97 (8) (2014) 2401–2404.
[14] A.A.N. Khoee, A. Habibolahzadeh, F. Qods, H. Baharvandi, Microstructure and properties of DCP-derived W-ZrC composite using nontoxic sodium alginate to fabricate WC preform, J. Mater. Eng. Perform. 24 (4) (2015) 1641–1648.
[15] T. Sato, A. Kochi, Y. Shirosaki, S. Hayakawa, M. Aizawa, A. Osaka, M. Kikuchi, Preparation of injectable hydroxyapatite/collagen paste using sodium alginate and influence of additives, J. Ceram. Soc. Jpn. 121 (1417) (2013) 775–781.
[16] Z.P. Xie, Y. Huang, Y.L. Chen, Y. Jia, A new gel casting of ceramics by reaction of sodium alginate and calcium iodate at increased temperatures, J. Mater. Sci. Lett. 20 (13) (2001) 1255–1257.
[17] A.P. Goswami, S. Roy, M.K. Mitra, G.C. Das, Impurity-dependent morphology and grain growth in liquid-phase-sintered alumina, J. Am. Ceram. Soc. 84 (7) (2001) 1620–1626.
[18] Y.-M. Kim, S.-H. Hong, D.-Y. Kim, Anisotropic abnormal grain growth in TiO2/SiO2-doped alumina, J. Am. Ceram. Soc. 83 (11) (2000) 2809–2812.
[19] P.Y. Hou, Impurity effects on alumina scale growth, J. Am. Ceram. Soc. 86 (4) (2003) 660–668.
[20] S.-J. Cho, Y.-C. Lee, H.-L. Lee, S.-M. Sim, M. Yanagisawa, Chemical inhomogeneity in commercial alumina powders and its effect on abnormal grain growth during sintering, J. Eur. Ceram. Soc. 23 (13) (2003) 2281–2288.
[21] G.R. Seely, R.L. Hart, Binding of aluminum and aluminum alizarin to alginate, Macromolecules 9 (3) (1976) 483–489.
[22] J.E. Gregor, E. Fenton, G. Brokenshire, P. Van Den Brink, B. O'Sullivan, Interactions of calcium and aluminium ions with alginate, Water Res. 30 (6) (1996) 1319–1324.
[23] A.R. Studart, V.C. Pandolfelli, E. Tervoort, L.J. Gauckler, Gelling of alumina suspensions using alginic acid salt and hydroxyaluminum diacetate, J. Am. Ceram. Soc. 85 (11) (2002) 2711–2718.
[24] J. Ma, Z. Xie, H. Miao, B. Zhang, X. Lin, Y. Cheng, Gelcasting of alumina ceramic components in nontoxic Na-alginate–CaIO3–PVP systems, Mater. Design 26 (4) (2005) 291–296.
[25] I. O. f. Standardization, ISO 4287, (1997).
[26] G.I.f. Standardisation, DIN EN 623-3, In Advanced technical ceramics—Monolithic ceramics; General and textural properties—Part 3: Determination of grain size and size distribution (characterized by the linear intercept method) (2003).
[27] G. Elssner, H. Hoven, G. Kiessler, P. Wellner, R. Wert, Material-specific preparation of polished sections, in: G.E.H.K.W. Wert (Ed.), Ceramics and Ceramic Composites, Elsevier Science, New York, 1999, pp. 59–133, Chapter 4.
[28] G.i.f. standardization, DIN EN 843-1. In Advanced technical ceramics—Mechanical properties of monolithic ceramics at room temperature—Part 1: Determination of flexural strength, (2008).
[29] R. Laucournet, C. Pagnoux, T. Chartier, J.-F. Baumard, Coagulation method of aqueous concentrated alumina suspensions by thermal decomposition of hydroxyaluminum diacetate, J. Am. Ceram. Soc. 83 (1) (2000) 2661–2667.
[30] J. Xu, N. Wen, H.X. Li, F. Qi, X.Q. Xi, J.L. Yang, Direct coagulation casting of alumina suspension by high valence counter ions using Ca(IO3)2 as coagulating agent, J. Am. Cerami. Soc. 95 (8) (2012) 2525–2530.
[31] B. Balzer, M.K.M. Hruschka, L.J. Gauckler, Coagulation kinetics and mechanical behavior of wet alumina green bodies produced via DCC, J. Colloid Interface Sci. 216 (2) (1999) 379–386.
[32] A.Y. Malkin, A.I. Isayev, 2-viscoelasticity, in: A.Y.M.I. Isayev (Ed.), Rheology Concepts, Methods, and Applications, Second edn., Elsevier, Oxford, 2012, pp. 43–126.
[33] I.-J. Bae, S. Baik, Abnormal grain growth of alumina, J. Am. Ceram. Soc. 80 (5) (1997) 1149–1156.
[34] S.I. Bae, S. Baik, Determination of critical concentrations of silica and/or calcia for abnormal grain growth in alumina, J. Am. Ceram. Soc. 76 (4) (1993) 1065–1067.
[35] A. Altay, M.A. Gülgün, Microstructural evolution of calcium-doped α-Alumina, J. Am. Ceram. Soc. 86 (4) (2003) 623–629.
[36] P. Sikorski, F. Mo, G. Skjåk-Bræk, B.T. Stokke, Evidence for egg-box-compatible interactions in calcium–alginategels from fiber X-ray diffraction, Biomacromolecules 8 (7) (2007) 2098–2103.
[37] J. Gurauskis, A.J. Sánchez-Herencia, C. Baudín, Joining green ceramic tapes made from water-based slurries by applying low pressures at ambient temperature, J. Eur. Ceram. Soc. 25 (15) (2005) 3403–3411.
[38] J. Gurauskis, A.J. Sánchez-Herencia, C. Baudín, Alumina–zirconia layered ceramics fabricated by stacking water processed green ceramic tapes, J. Eur. Ceram. Soc. 27 (2,3) (2007) 1389–1394.
[39] J.-H. Han, Joining partially-sintered alumina ceramics using a mixture slurry of alumina sol and suspension, Ceram. Int. 40 (2) (2014) 3123–3129.
[40] J.-H. Han, Joining alumina ceramics in green state using a paste of ceramic slurry, J. Mater. Process. Technol. 211 (6) (2011) 1191–1196.
[41] H. Miyazaki, M. Hotta, H. Kita, Y. Izutsu, Joining of alumina with a porous alumina interlayer, Ceram. Int. 38 (2) (2012) 1149–1155.
[42] L. Wang, F. Aldinger, Joining of advanced ceramics in green state, Mater. Lett. 54 (2,3) (2002) 93–97.
[43] A. Krell, P. Blank, H. Ma, T. Hutzler, M. Nebelung, Processing of high-density submicrometer Al2O3 for new applications, J. Am. Ceram. Soc. 86 (4) (2003) 546–553.
[44] J. Ma, Z. Xie, H. Miao, Y. Huang, Y. Cheng, W. Yang, Gelcasting of alumina ceramics in the mixed acrylamide and polyacrylamide systems, J. Eur. Ceram. Soc. 23 (13) (2003) 2273–2279.